Title

In vivo manipulation of the extracellular matrix induces vascular regression in a basal chordate

Journal

Molecular Biology of the Cell, 28(14)

ISSN

1059-1524

Authors

Rodriguez, Delany

Braden, Brian P

Boyer, Scott W

et al.

Publication Date

2017-07-07

DOI

10.1091/mbc.e17-01-0009

Peer reviewed

In vivo manipulation of the extracellular matrix induces vascular regression in a basal chordate

Delany Rodriguez[a,†], Brian P. Braden[a,†], Scott W. Boyer[a], Daryl A. Taketa[a], Leah Setar[a], Chris Calhoun[a], Alessandro Di Maio[a], Adam Langenbacher[a], Megan T. Valentine[b], and Anthony W. De Tomaso[a,*]

[a]Department of Molecular, Cellular and Developmental Biology and [b]Department of Mechanical Engineering, University of California, Santa Barbara, Santa Barbara, CA 93106

ABSTRACT **We investigated the physical role of the extracellular matrix (ECM) in vascular homeostasis in the basal chordate *Botryllus schlosseri*, which has a large, transparent, extracorporeal vascular network encompassing an area >100 cm^2. We found that the collagen cross-linking enzyme lysyl oxidase is expressed in all vascular cells and that in vivo inhibition using β-aminopropionitrile (BAPN) caused a rapid, global regression of the entire network, with some vessels regressing >10 mm within 16 h. BAPN treatment changed the ultrastructure of collagen fibers in the vessel basement membrane, and the kinetics of regression were dose dependent. Pharmacological inhibition of both focal adhesion kinase (FAK) and Raf also induced regression, and levels of phosphorylated FAK in vascular cells decreased during BAPN treatment and FAK inhibition but not Raf inhibition, suggesting that physical changes in the vessel ECM are detected via canonical integrin signaling pathways. Regression is driven by apoptosis and extrusion of cells through the basal lamina, which are then engulfed by blood-borne phagocytes. Extrusion and regression occurred in a coordinated manner that maintained vessel integrity, with no loss of barrier function. This suggests the presence of regulatory mechanisms linking physical changes to a homeostatic, tissue-level response.**

Monitoring Editor
Valerie Marie Weaver
University of California, San Francisco

Received: Jan 9, 2017
Revised: Jun 5, 2017
Accepted: Jun 5, 2017

INTRODUCTION

Epithelial tissues are associated with a layer of specialized extracellular matrix (ECM) called the basement membrane, which functions as a structural support and is a source of molecular signals that regulate growth and homeostasis (Brown, 2011). Development of tubular organs, including the vasculature, lungs, and endocrine glands, includes expansion of epithelial tubes in a process called branching morphogenesis, which includes extensive remodeling of the basement membrane to allow it to remain associated with the cells as they grow, while localized changes in structure provide physical cues for growth and morphogenesis (Rozario and DeSimone, 2010). In many cases, after embryogenesis, tubular organs cyclically grow and regress over the lifetime of an individual. For example, the mammalian breast glands undergo dramatic changes during pregnancy: initially quiescent tissue is induced to proliferate and form milk-producing alveoli, and, after weaning, these structures regress via a controlled apoptotic mechanism called involution. Both processes require extensive remodeling of the ECM to accommodate expansion and regression (Macias and Hinck, 2012), but the molecular mechanisms that regulate and integrate remodeling with expansion and contraction of an epithelium are not well understood.

We are investigating the role of the ECM during branching morphogenesis and homeostasis in the extracorporeal vasculature of the colonial ascidian *Botryllus schlosseri.* Ascidians are marine invertebrate chordates that are the closest nonvertebrate relatives of vertebrates (Delsuc *et al.*, 2006). *Botryllus* belongs to a subset of ascidians that are colonial and grow via a recurring asexual budding process that gives rise to a colony of genetically identical individuals (called zooids). The zooids are connected by an extensive extracorporeal vascular network that consists of large vessels (~0.25-mm diameter) that ramify throughout the colony and can cover areas >100 cm^2. At the periphery of the colony, the vessels terminate in

This article was published online ahead of print in MBoC in Press (http://www.molbiolcell.org/cgi/doi/10.1091/mbc.E17-01-0009) on June 14, 2017.

†These authors contributed equally to this work.

*Address correspondence to: Anthony W. De Tomaso (detomaso@lifesci.ucsb.edu).

Abbreviations used: BAPN, β-aminopropionitrile; ECM, extracellular matrix.

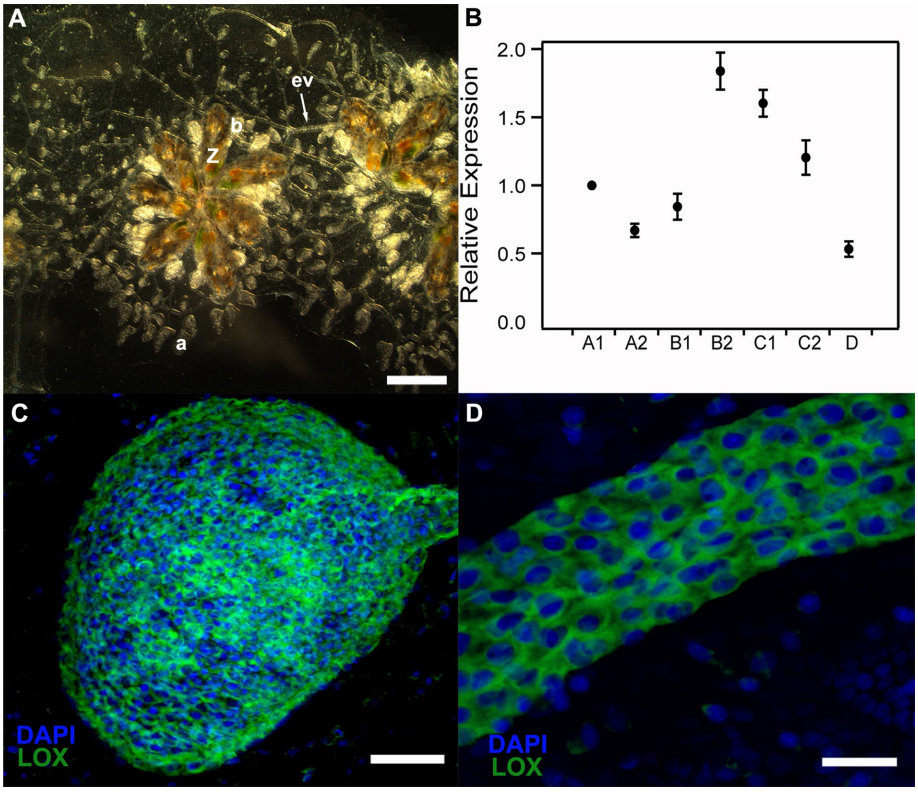

FIGURE 1: LOX1 is expressed by vasculature tissue. (A) Light micrograph of a *Botryllus* colony. The zooids (Z) and buds (b) arrange themselves into star-shaped structures called systems. A colony can consist of multiple systems, all connected by a large common extracorporeal vasculature (ev). At the periphery of the colony, the vasculature terminates in sac-like appendages called ampullae (a). (B) Relative expression of LOX1 during the asexual cycle normalized to stage A1. (C, D) Fluorescence in situ hybridization of the *B. schlosseri* homologue of *lysyl oxidase* (*LOX1*), showing expression of *LOX1* in both ampullae (C) and the marginal vessel (D) of the extracorporeal vasculature tissue. Scale bars, 2 mm (A), 50 µm (C, D). Negative control using a sense probe is shown in Supplemental Figure S1.

sac-like structures called ampullae (Figure 1A). The zooids and vasculature are embedded within a structure called the tunic, a thin, transparent matrix that consists of both cellulose and proteins (Brunetti and Burighel, 1969; Burighel and Brunetti, 1971; Patricolo and Ferrarella, 1973; Vizzini *et al.*, 2002; Gasparini *et al.*, 2007).

Although *Botryllus* is a chordate, the structure of the blood vessels is inverted in comparison to mammals. Rather than a mesoderm-derived endothelium, vessels are constructed of ectoderm-derived epithelium, with the basal lamina lining the vessel lumen and the apical side facing outward, into the tunic. In addition to being large and existing outside the body, the vessels are also sessile and transparent. Experimentally, these anatomical characteristics allow direct access to the basement membrane via microinjection, as well as the ability to live-image and directly physically manipulate the vessels. In addition, we have developed a fluorescent lineage-tracing methodology that allows isolation of pure populations of vascular cells by flow cytometry (Braden *et al.*, 2014).

The extracorporeal vascular network of *Botryllus* is a highly dynamic tissue. A *Botryllus* colony grows via weekly rounds of asexual budding, and, depending on environmental conditions, the colony can quadruple in size every week, requiring ongoing expansion of the vascular network for the life of the individual.

In addition, the vasculature is highly regenerative: after surgical ablation, the entire network will regrow in ~72 h (Tiozzo *et al.*, 2008). Finally, under normal conditions, some vessels actively remodel and extend and retract several millimeters over 24- to 48-h periods. These characteristics allow us to study the morphogenesis and maintenance of epithelial tubes in a functioning vascular network in vivo during both normal and induced angiogenesis, as well as involution of the vascular network.

Here we focus on the dynamics of the basement membrane and the interplay between vascular cells and the ECM components that underlie continuous angiogenesis in *Botryllus*. We found that a lysyl oxidase 1 (LOX1) homologue in *Botryllus* is highly expressed during the entire asexual cycle and hypothesized that it could play a role in vascular homeostasis (Figure 1B). In vertebrates, LOX1 is secreted by a number of tissues, including blood vessels, and plays a critical role in modifying the basement membrane by cross-linking collagen and elastin, thus controlling the stiffness of the ECM (Bignon *et al.*, 2011; Chen *et al.*, 2013, 2015; Cox *et al.*, 2015; Liu *et al.*, 2015; Wang *et al.*, 2016). Disruption of LOX activity can affect multiple tissues, including blood vessels, lungs, bone, and ligaments, and can increase the risk of aortic aneurysms (Smith-Mungo and Kagan, 1998).

When we blocked LOX activity in vivo using the specific pharmacological inhibitor β-aminopropionitrile (BAPN), we found that it caused global regression of the blood vessels within 16 h, without any evident pathology such as bleeding or plasma leakage. Using a combination of live imaging, flow cytometry, and small-molecule inhibitors, we determined that regression is due to apoptosis and extrusion of the cells from the vessel wall, followed by phagocytosis of the cell corpses. BAPN treatment changed collagen structure in the blood vessels, and regression could also be induced by blocking focal adhesion kinase (FAK) and Raf activity using small-molecule inhibitors, suggesting that BAPN-induced changes were detected by differences in integrin binding. The results taken together suggest that the ECM of the vessels is in a highly dynamic state that requires constant cross-linking and that changes in the physical environment induce a tissue-level response.

RESULTS

The collagen cross-linking protein LOX1 is expressed by vascular cells

Analysis of an mRNA-sequencing database (Rodriguez *et al.*, 2014) revealed that four LOX homologues were expressed in *Botryllus*, including one LOX1-, two LOX3-, and one LOX4-like genes. The *Botryllus* LOX1 gene was highly homologous to mammalian LOX genes (*E*-value < 1e-39), and quantitative PCR (qPCR) analysis revealed a nearly constant level of expression throughout the life cycle (Figure 1B). Next the spatial expression pattern was determined using whole-mount in situ hybridization with a *Botryllus* LOX1–specific probe, which revealed high levels of expression by all cells of the extracorporeal vascular tissue, including both peripheral ampullae (Figure 1C) and marginal blood vessels (Figure 1D). The specificity of the antisense probe was confirmed by using a control sense

probe that showed no signal on either ampullae or blood vessels (Supplemental Figure S1, A and B).

Inhibition of LOX activity induces global and reversible vascular regression

To assess the role of LOX activity in vivo, we used BAPN, a specific inhibitor of lysyl oxidase activity (Kagan, 2000). When colonies were transferred to seawater containing BAPN and incubated, we discovered a completely unexpected and highly robust phenotype. Within a few hours of BAPN exposure, the entire extracorporeal vasculature began to regress, with all vessels simultaneously retracting toward the center of the colony (Figure 2, A and B, and Supplemental Video S1). This regression event was rapid: within the 16 h of total incubation time, all of the vessels had withdrawn underneath the zooids, a distance of nearly 10 mm for some of the vessels (Figure 2, A and B). Of importance, time-lapse microscopy showed that vascular regression occurred without pathology: no bleeding or plasma leakage was observed, indicating that the vessels regressed while maintaining barrier function (Supplemental Video S1). Regression of the vascular bed occurred within the tunic, and the tunic remained intact with no observable changes (Figure 2B). The BAPN response was also reversible: after removal of BAPN, vessels began to regrow, eventually restoring the vascular bed to its original size (Supplemental Figure S2). Finally, during BAPN treatment, the zooids continued to function normally, including continuously feeding and defecating, with no observable changes in the heart rate, and undergoing blastogenesis at a normal pace. To assess whether the tunic cells are affected by BAPN treatment, we incubated colonies for 8 h in BAPN and then fixed and stained with phalloidin. No changes in the tunic or tunic cells were observed between BAPN-treated and control colonies (Supplemental Figure S3).

To determine whether there was a dose-dependent response to BAPN, we quantified changes in the distal circumference of the extracorporeal vasculature 16 h after treatment with different concentrations of BAPN (0 [control], 50, 100, 200, and 400 µM). The results, shown in Figure 2, A and B, demonstrate that the global regression correlated to BAPN concentrations between 50 and 400 µM (Figure 2C). BAPN doses >400 µM (800 µM, 1 mM, and 5 mM) also induced a reversible regression within 4 h but were lethal in incubations >8 h.

Regressed vasculature exhibits gross morphological changes

We next characterized the morphological changes in vascular tissue that occur upon BAPN treatment as compared with untreated tissue. Using our previously described technique of labeling vascular tissues using acid-stable fluorophores (Braden *et al.*, 2014), we labeled the vasculature and induced vascular regression using BAPN treatment (Figure 3, A–D). Using time-lapse fluorescence microscopy, we observed gross morphological changes to the vascular tissues. In general, vessels appeared less rigid and seemed deflated, and although some regions of bulging were also observed. The morphology of the ampullae also changed, becoming thinner and deflated during regression (Figure 3, B–D) compared with the cylindrical appearance of ampullae in controls (Figure 3A).

We next used transmission electron microscopy (TEM) to assess BAPN-induced changes at the ultrastructural level (Figure 4). Figure 4, A and A′, shows representative images of the basement membrane for an unmanipulated colony. At high magnification (Figure 4A′), we observed that the basement membrane contains long and short fibrils with a quarter-stagger segmented staining pattern, typical of collagen fibers, intercalating with one another and forming thin bundles on the lumen side of the vessel. These structures are clearly affected by BAPN treatment (Figure 4B). Within bundles, collagen fibers seem to be disrupted, with no clear organization and structure (Figure 4B′, inset), and there is a loss of quarter-stagger staining. These results were corroborated using second-harmonic imaging (SHI), which allows high-sensitivity imaging of collagen fibers (Cox *et al.*, 2003; Campagnola, 2011; Chen *et al.*, 2012). In these experiments, control and BAPN-treated colonies were fixed at 0, 8, and 16 h after drug administration and analyzed by SHI. In controls, collagen fibers can be detected at all time points (Figure 4, C–E and I), whereas in BAPN-treated colonies, we detected a loss a fiber content by 8 h and a dramatic drop of detectable signal 16 h after initiation of BAPN treatment (Figure 4, F–H and I). Given that the role of LOX is to modify lysine residues in the collagen protein, which then form spontaneous cross-linkages, inhibition should not directly affect preexisting fibers but only prevent assembly and stabilization of new fibrils. Thus the rapid and specific changes seen in BAPN-treated colonies and the reversibility of its effects suggest that

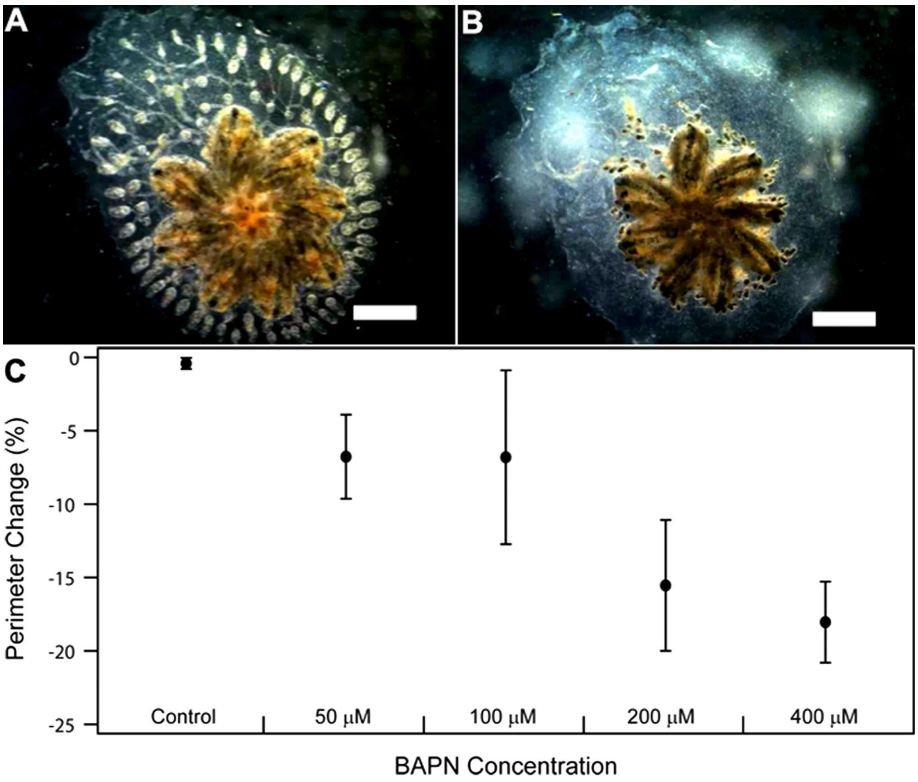

FIGURE 2: BAPN induces regression of the extracorporeal vasculature. (A) Dorsal view of *B. schlosseri* colony before BAPN treatment and (B) after 16 h of 400 µM BAPN treatment. The vessels have withdrawn underneath the colony (also see Supplemental Video S1). (C) BAPN dose–response curve. Changes in the vascular perimeter were assessed 16 h after BAPN exposure. Scale bars, 2 mm.

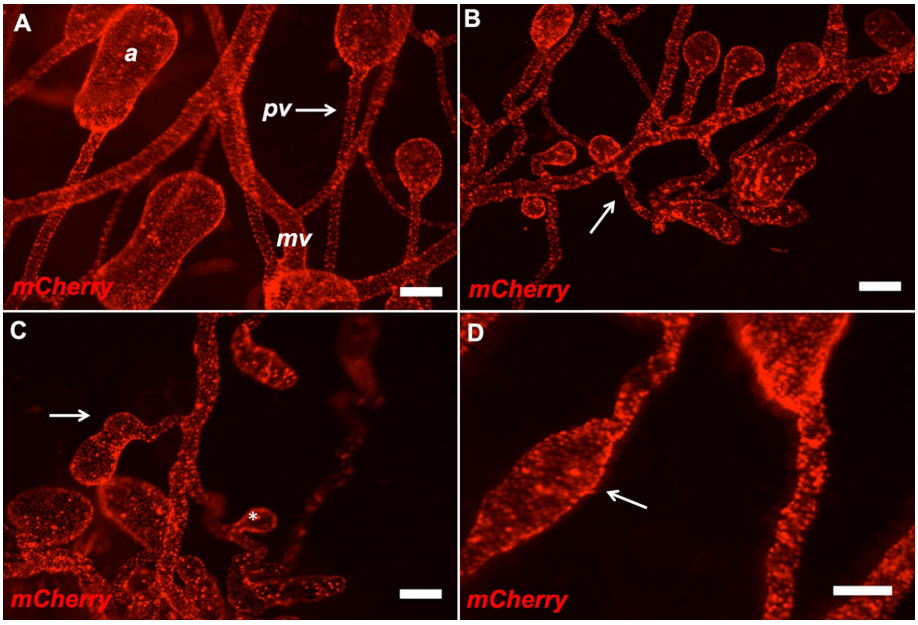

FIGURE 3: Gross changes in vascular morphology after BAPN treatment. (A) Fluorescently labeled extracorporeal vasculature showing ampullae (a), peripheral vessels (pv), and marginal vessels (mv) in a control *B. schlosseri* colony and (B) after BAPN treatment. The regressed vasculature contains shorter peripheral vessels (arrow) between the ampullae and marginal vessels. (C, D) Close-up views of gross changes in ampullae morphology, including bulging (arrows), and deflation (asterisk). Scale bars, 100 μm.

the basement membrane of the blood vessels is highly dynamic and is in a constant state of remodeling, even under normal conditions.

BAPN treatment induces apoptosis in a subset of vascular cells

The scale of vessel withdrawal suggested that regression must involve removal of cells from the vessel walls. Further, because collagen disruption triggered the withdrawal, we hypothesized that vessel regression was due to anoikis: apoptosis induced by the loss of cell/ECM interactions (Frisch and Francis, 1994), followed by cell extrusion and removal. To identify and characterize apoptosis within the vasculature, we used fluorescently labeled annexin V (Figure 5), which binds phosphatidylserine after translocation to the extracellular membrane leaflet, an event that occurs early in apoptosis and targets cells for phagocytosis (Guo *et al.*, 2013; Li *et al.*, 2013; Wu *et al.*, 2013; Zang *et al.*, 2014). These experiments were performed in vivo and in real time, allowing the dynamic cellular changes driving regression to be directly observed (Figure 5, A–D). Labeled annexin V was injected into the vasculature, and its binding to cells was assessed with fluorescence microscopy in control conditions or after exposure to BAPN. By 16 h, we observed an 8- to 10-fold increase in annexin V+ cells after BAPN treatment compared with control conditions (Figure 5E). We independently confirmed this increase using fluorescence-activated flow cytometry (FACS) to separate annexin V+ from annexin V– vascular cells after the same treatments (Figure 5F). BAPN treatment induced a nearly equivalent fivefold increase in annexin V+ cells after BAPN incubation, as detected by FACS.

An alternative hypothesis is that vascular regression was due to shrinkage of cells within the blood vessels. We assessed this qualitatively by staining fixed vascular tissues with fluorescent phalloidin, which allowed us to visualize the cell boundaries through labeling of the actin cortices of each cell. We compared colonies 8 h after BAPN treatment, when regression is maximal, to untreated controls. As shown in Supplemental Figure S4, BAPN does not cause gross changes to cell size that could account for the regression phenotype. Thus we conclude that vascular regression induced by BAPN results from extrusion, not shrinkage, of vascular cells.

Apoptotic vascular cells are extruded basolaterally while being ingested by blood-based phagocytes

We did not observe labeled vascular cells in the circulation or tunic during regression, so we next investigated the role of phagocytic cells in vascular cell apoptosis. Blood-based phagocytic cells in *Botryllus* have been characterized and can be selectively labeled through injection of fluorescent BioParticles into the vasculature, which allows detection in vivo for up to 2 wk (Lauzon *et al.*, 2013). To assess the interactions between the vascular and phagocytic cells, we injected *Botryllus* colonies with Alexa Fluor 647–conjugated bovine serum albumin (BSA) to label vascular cells and Alexa Fluor 488–conjugated BioParticles to label phagocytic cells. Control and BAPN-treated labeled colonies were monitored over the course of 16 h using fluorescence time-lapse microscopy. As shown in Figure 6, phagocytosis of labeled vasculature occurred at a significantly higher rate after BAPN treatment, as determined by a large increase in double-labeled phagocytic cells in the blood (Figure 6, A and B). This suggested that apoptotic vascular cells were extruded from the vessel wall, through the basal lamina, and then immediately engulfed by phagocytes. Next we live imaged vessels during regression (Figure 7 and Supplemental Video S2) to visualize the potential coordination of cell extrusion and phagocytosis. In this experiment, the entire colony was soaked with the lipophilic dye CellMask (green), which primarily labeled the vessel epithelial cells, as well as accessory cells in the tunic (asterisks), with some label penetrating and labeling some individual blood cells (Figure 7, A–D). In addition, phagocytic cells were labeled with BioParticles (red; Figure 7, A–D). In still images from this movie, a large phagocyte can be seen moving with the circulation (Figure 7A), stopping directly underneath a vascular cell (arrow; Figure 7B), engulfing it (Figure 7C), and then returning to the circulation (Figure 7D). Given that regression occurs without loss of barrier function and we did not observe labeled vascular cells in the circulation, this suggests that the phagocyte may play a role in the extrusion event itself.

BAPN treatment blocks phosphorylation of FAK

Treatment by BAPN disrupts the structure of the collagen fibrils in the basement membrane, suggesting that cells might be dying due to loss of tonic survival signaling from integrin binding. To directly investigate this, we next assessed the role of integrin signaling pathways during regression, focusing first on the function of FAK, a cytoplasmic tyrosine kinase phosphorylated by integrin stimulation. FAK is expressed in the transcriptome of FACS-isolated vascular cells (unpublished data).

Experimentally, colonies were incubated in filtered sea water (FSW) containing a chemical inhibitor of FAK (FAKI14; see *Materials and Methods*), which blocks autophosphorylation of FAK Y397 and

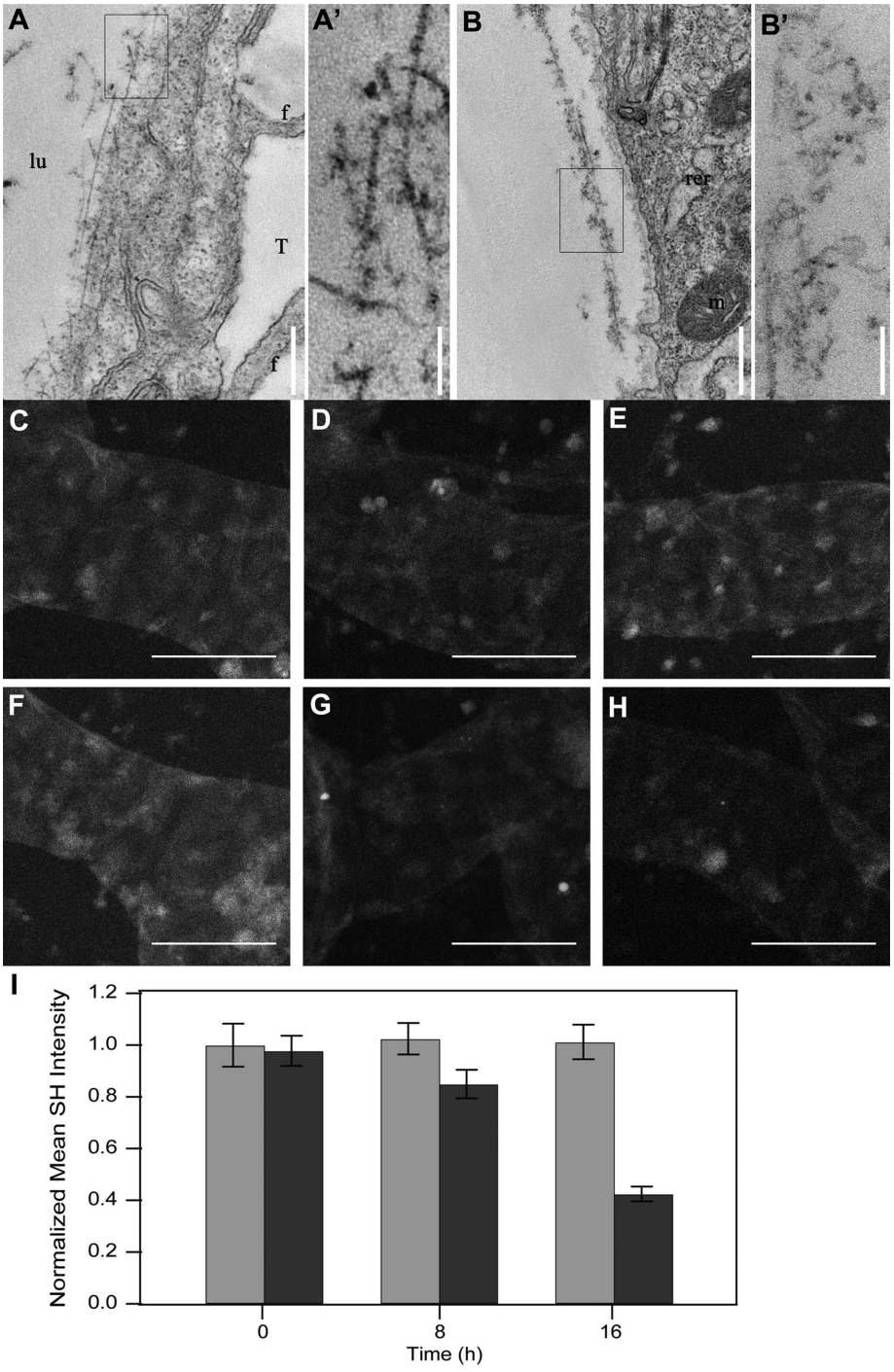

FIGURE 4: BAPN treatment induces changes in collagen structure. Transmission electron micrographs of vascular cells showing a significant difference in the collagen organization and structure (insets A′ and B′) of the extracorporeal vascular tissue between control (A) and BAPN-treated animals (B). BAPN treatment clearly changes in quarter-stagger collagen fibril staining (compare A′ to B′). f, filopodia; lu, lumen; m, mitochondria; rer, rough endoplasmic reticulum; T, tunic. (C–H) Second harmonic imaging of collagen fibers of vascular tissue. Control vessels at 0 (C), 8 (D), and 16 (E) h, showing no changes in collagen fiber detection. BAPN-treated vessels at 0 (F), 8 (G), and 16 (H) h show a decrease in collagen fiber detection over time. (I) Quantification of signal intensity shown as corrected total signal and normalized to control at 0 h, showing a significant decrease in signal on BAPN treated vessels at 8 and 16 h. Scale bars, 500 nm (A, B), 100 nm (A′, B′), 50 μm (C–H).

downstream interactions with Src and phosphoinositide 3-kinase, an initial step in the canonical integrin signaling pathway (Hochwald *et al.*, 2009). We found that FAKI14 treatment induced regression with equivalent kinetics and circumference changes to those observed after treatment with BAPN, with no loss of vessel barrier function (Supplemental Figure S5). In addition, FAKI14-induced changes were also reversible and dose dependent (unpublished data).

To assess the specificity of FAKI14, we quantified levels of phosphorylated Y397 FAK using a phosphospecific monoclonal antibody in an intracellular phospho flow assay. Briefly, the vasculature was fluorescently labeled, and single-cell suspensions were prepared from untreated and BAPN-treated colonies. After fixation, vascular cells could readily be identified from non-vascular tissue using flow cytometry (Figure 8A). The level of FAK phosphorylation within the vascular cells subset was reliably quantifiable (Figure 8, B and C), and treatment with FAKI14 resulted in a greater than twofold reduction in antibody signal compared with controls (Figure 8B). The anti-FAK pY397 antibody also immunoprecipitates and detects a protein of the correct molecular weight via Western blotting (Supplemental Figure S5E).

If BAPN-induced vascular regression is due to anoikis via changes in integrin binding, then BAPN treatment should also affect FAK signaling. We next quantified the changes in pY397 FAK levels in vascular cells during BAPN treatment compared with untreated colonies. High levels of pY397 FAK were present in 69% (±7%) of untreated vascular cells (Figure 8C). In contrast, there was a dose-dependent loss of pY397 FAK in cells treated with BAPN (Figure. 8C). After 4 h, high concentrations of BAPN induced a similar reduction in phosphorylated FAK (37 ± 9%) compared with the FAK14 inhibitor (33 ± 3%; $p = 0.02$).

Finally, we investigated the role of Raf kinase in the regression process. Raf is also highly expressed in the transcriptome of FACS isolated vascular cells (unpublished data), and we found that inhibition of Raf kinase signaling using a small-molecule inhibitor also induced a dose-dependent, reversible regression (Supplemental Figure S5). In agreement with the canonical integrin-signaling cascade where Raf is downstream of FAK (Morse *et al.*, 2014), we found that Raf-induced regression did not alter FAK phosphorylation levels (Figure 8C). In summary, small-molecule inhibitors of FAK and Raf both induce a regression phenotype that phenocopies BAPN treatment, and pY397 FAK levels correlate to the location of the inhibitor targets in the canonical integrin-signaling pathway. Together, these data suggest that BAPN-induced changes in collagen structure induce anoikis via changes in integrin binding.

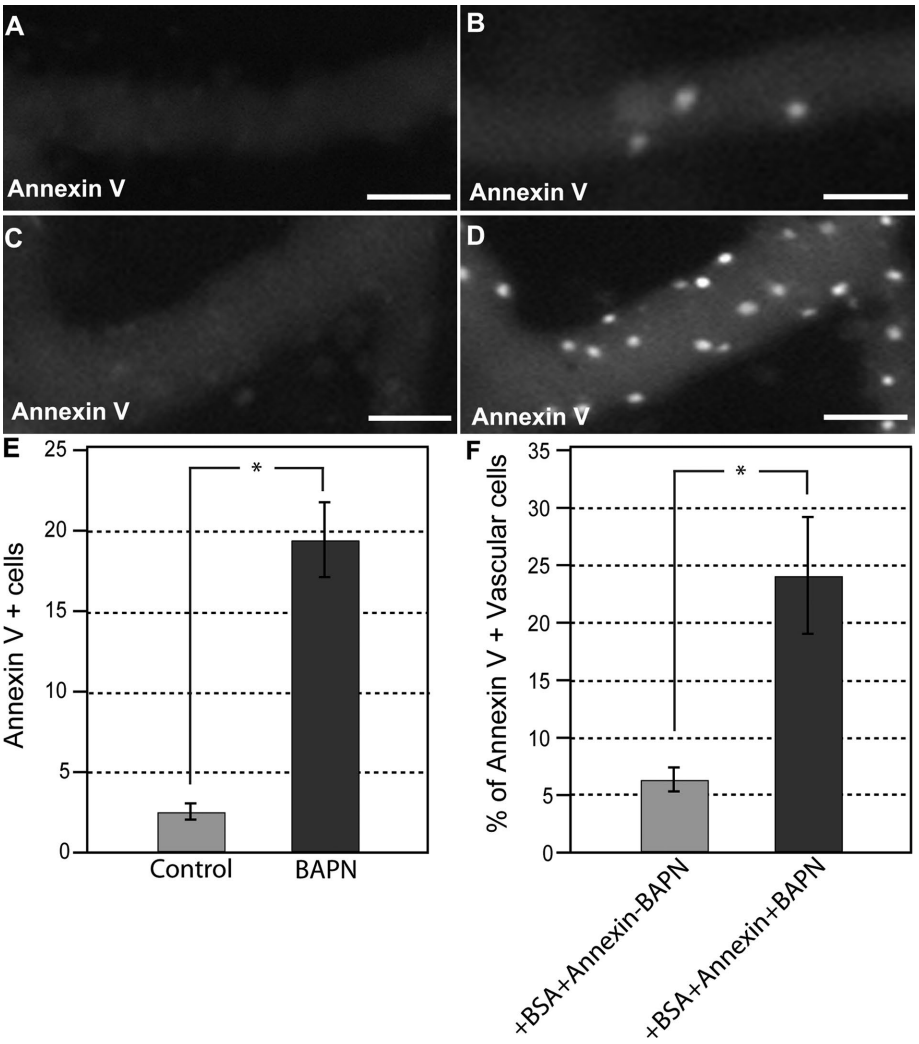

FIGURE 5: Regressing vasculature contains increased apoptotic cells. (A–D) Detection of apoptotic cells using fluorescently labeled annexin V. (A) Confocal micrograph of a region of the extracorporeal vasculature of a control colony immediately after injection and (B) 16 h later. (C) Confocal micrograph of the extracorporeal vasculature of a control colony immediately after BAPN injection and (D) 16 h after treatment, showing an increased number of apoptotic cells. (E) Quantification of annexin V–fluorescein isothiocyanate–positive cells in control and BAPN-treated colonies after 16 h; $p = 0.001$. (F) Quantification of apoptotic cells in the vasculature by FACS. BSA-488–labeled colonies were injected with fluorescently labeled annexin V, followed by treatment with BAPN. Cells were isolated immediately after initiation of BAPN treatment (gray bar) or 16 h after incubation (black bar), and the percentage of BSA-488+/annexin V+ cells was determined by FACS. Scale bars, 50 μm (A–D).

DISCUSSION

Here we show that inhibition of LOX activity rapidly changes the structure of the vascular basement membrane and induces apoptosis in vascular cells in a manner that correlates to changes in the levels of pY397 FAK. Regression can also be induced using inhibitors of FAK and Raf, key proteins in the canonical integrin-signaling cascade (Guo and Giancotti, 2004). Cells are extruded through the basement membrane and immediately engulfed by blood-borne phagocytic cells. Taken together, our results suggest that manipulation of the stiffness of the basement membrane is detected by changes in integrin signaling, inducing anoikis in vascular cells. Regression occurs in a coordinated manner that maintains vessel integrity, suggesting that BAPN treatment is triggering either a homeostatic or normal physiological process but on a global scale. In summary, we are observing a coordinated, tissue-level response to a disruption in the physical environment detected by integrin signaling.

Dynamics of the basement membrane

We determined that *LOX1* expression is constant and ubiquitous in the *Botryllus* vascular cells, suggesting that the protein plays an important role in homeostasis of its vasculature. In adult mammals, BAPN treatment induces thoracic aortic aneurysms and dissection, demonstrating that cross-linking of the vascular ECM by LOX is required for vascular homeostasis (Maki *et al.*, 2002), and LOX activity has also been shown to be involved in collagen IV assembly during angiogenesis in zebrafish (Bignon *et al.*, 2011). The very rapid response to BAPN treatment in *Botryllus* was not expected, although in retrospect it may not be surprising. The inverted anatomy of the *Botryllus* vessels provides unrestricted access to the entire basement membrane, and by soaking a whole animal in the drug, we allow nearly immediate interaction between the enzyme and inhibitor along the entire vascular network. This allows us to decouple the time scales of BAPN delivery (which in our system is nearly instantaneous) and BAPN action.

In addition, the vasculature and associated basement membrane in *Botryllus* are not static structures. *Botryllus* grows by asexually expanding over the substrate and has the potential to double or even quadruple in size every week. Time-lapse videos reveal that individual vessels in control animals extend and retract by several millimeters over 24- to 48-h-long time scales. Thus the vasculature is never in a globally quiescent state; instead, it exists in a constant state of localized extension and involution. In addition, the basement membrane lines the lumen of the vessel and thus is subjected to constant shear forces, which may require constant remodeling activity. The results taken together suggest that the basement membrane in *Botryllus* may be constantly in a state analogous to the provisional ECM that stimulates angiogenesis in vertebrates (Senger and Davis, 2011). We recently completed our initial mRNA-sequencing analysis of FACS-purified vascular cells under control conditions, and they have high expression of ECM remodeling proteins such as matrix metalloproteinases (MMPs), disintegrin and metalloproteinases (ADAM), and disintegrin and metalloproteinases with thrombospondin repeats (ADAMTS), and mephrins (unpublished data), consistent with these results.

A notable aspect of the ECM in the *Botryllus* vascular system is the presence of collagen fibrils in the basement membrane. Although this is unusual, there are other examples, including the basement membrane of the *Drosophila* egg chamber, in which fibril deposition was recently shown to play an important role in morphogenesis (Pastor-Pareja and Xu, 2011; Isabella and Horne-Badovinac, 2015).

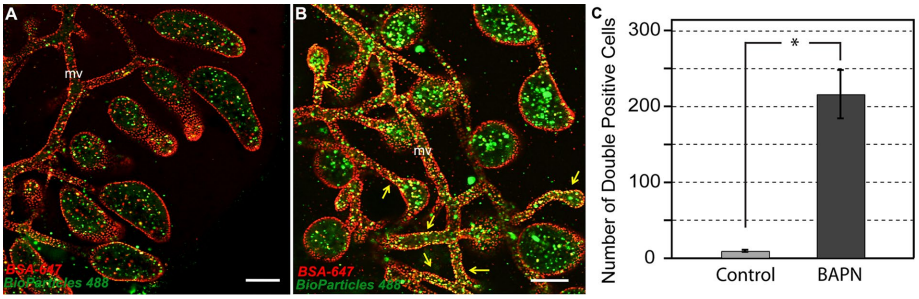

FIGURE 6: Basal extrusion and phagocytosis of vascular cells causes regression. (A) A region of the extracorporeal vasculature of a control colony. Circulating phagocytic cells are labeled using BioParticle-488 (green), and vascular cells are labeled using Alexa Fluor 647–conjugated BSA (red). Both marginal vessels (mv) and peripheral ampullae (a) can be seen in this field. (B) After BAPN treatment, basal extrusion and phagocytosis can be seen as colocalization of the labels in the circulating phagocytic cells (yellow arrows). Single-labeled vascular cells are not observed in the circulation after BAPN treatment. (C) Quantification of double-positive cells (BSA-647 and BioParticles) in control and BAPN-treated colonies. Statistical analysis was performed using Student's *t* test. $*p < 0.05$. Scale bars, 100 μm (A, B).

Finally, whereas branching morphogenesis is driven in part by localized changes in the ECM (Ihara *et al.*, 2011; Harunaga *et al.*, 2014; Morrissey and Sherwood, 2015), in *Botryllus* this occurs in an inverted manner, with the ECM behind and following the new branch points instead of leading them. In summary, the accessibility of the basement membrane in *Botryllus*, coupled to a tissue that is already undergoing constant remodeling, likely underlies the rapid response to BAPN treatment and provides a novel visual assay to dissect the interactions between cells and the ECM during branching morphogenesis and regression.

Importance of integrin signaling to vascular remodeling

We have not yet demonstrated a direct link between integrin binding and levels of pY397 FAK. However, the fact that the level of pY397 FAK is correlated with the concentration of BAPN and the level of pY397 FAK does not change when regression is induced by the downstream inhibition of Raf is strong evidence that apoptosis is due to physical changes in the ECM detected by integrins. In addition, studies in *Botryllus* using small-molecule inhibitors for both Wnt and transforming growth factor β signaling produced phenotypes in the developing zooids but did not induce vascular regression, indicating that we are inhibiting canonical integrin signaling pathways in the present studies (Di Maio *et al.*, 2015; Langenbacher and De Tomaso, 2016).

We attempted to assess directly the role of integrin binding by injecting RGD-containing peptides, but results were not consistent. This was not surprising because peptides were injected into the active circulatory system and likely rapidly diluted, compromising their effects. In future studies, quantitative proteomics approaches using FACS-isolated vascular cells will allow us to assess directly changes in the proteome and phosphoproteome under different perturbations, dissect the pathways linking integrin binding to the induction of anoikis, and detect differences between apoptotic and nonapoptotic cells.

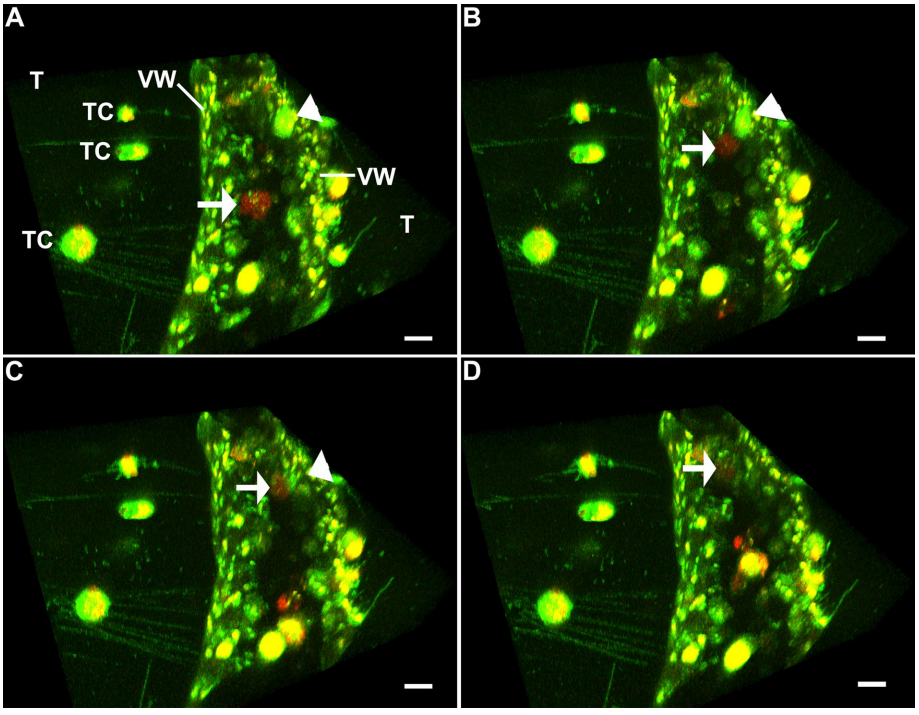

FIGURE 7: Vascular cells are engulfed by phagocytes in situ. Confocal images from a time-lapse video (Supplemental Video S2) of a blood vessel labeled with CellMask (green) and phagocytic cells labeled with BioParticles (red), showing engulfment of a vascular cell by a phagocyte. (A) Red-labeled phagocyte traveling through the bloodstream. (B) Phagocyte stops in front of a vascular cell. (C) Phagocyte engulfs vascular cell in situ. (D) After engulfment is completed, the phagocyte continues traveling through the bloodstream. Arrow indicates phagocyte, and arrowhead indicates the position of the vascular cell before and after engulfment. T, tunic; TC, tunic cell; VW, vessel wall. Scale bars, 10 μm.

Coordination of basal extrusion

The three inhibitors used in this study were all administered globally, so it is unclear why apoptosis is triggered in only a subset of cells. Understanding whether the distribution of apoptotic cells is random or not and, in the latter case, what selection process is used to induce apoptosis is critical to understanding how regressing vessels can maintain barrier function during withdrawal. It is possible that there is heterogeneity among the vessel cells in terms of the number of contacts with the ECM and other cells, making some more (or less) susceptible to anoikis. For example, it has been demonstrated that cells with low expression of the protein Merlin have higher FAK inhibitor sensitivity due to weaker cell–ECM and cell–cell contacts (Shapiro *et al.*, 2014), making these cells more sensitive to changes in FAK signaling. If epithelial cell survival requires a threshold value in terms of number or strength of cell–matrix and cell–cell contacts, then heterogeneity in these contacts along the vascular epithelium may make some more (or less) sensitive to BAPN and FAK inhibitor treatment. However, whereas heterogeneity could explain why some cells

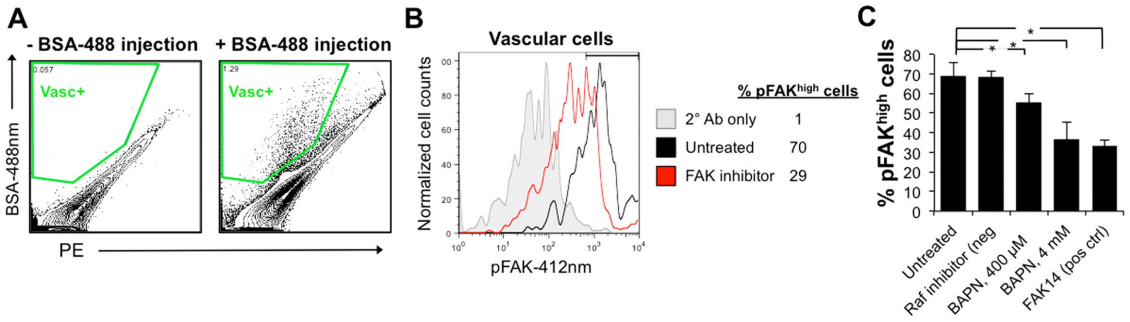

FIGURE 8: Disruption of collagen matrix by BAPN results in loss of integrin signaling in vascular cells. (A) Flow cytometry gating strategy for BSA-488–labeled *B. schlosseri* vascular cells after formaldehyde fixation and methanol permeabilization. (B) Representative flow cytometry histogram for quantifying phosphorylated Y397 FAK (pY397FAK) in *B. schlosseri* vascular cells. FAK inhibitor (FAK14) was used a positive control for blocking FAK phosphorylation. (C) Percentage of vascular cells with high FAK phosphorylation for *B. schlosseri* colonies after indicated treatment for 4 h ($n = 3$ per condition). *$p < 0.05$ as determined by an unpaired Student's *t* test.

would die 2 h after the initiation of treatment and others at 8 h, it does not explain how regression is coordinated. One of the most puzzling aspects of these studies is that global interference of integrin signaling, either by disrupting collagen structure or using inhibitors, is dose dependent but never to the point at which they affect each cell equally. We are observing a tissue-level response to a physical disruption, but the regulatory mechanisms that maintain epithelial homeostasis during regression are not clear.

One explanation for the global response is that changes in collagen structure cause a global release of tension that results in cells sensing that they are overcrowded. This could also trigger cell extrusion, a homeostatic response to crowding in epithelia that could explain maintenance of barrier function (Macara *et al.*, 2014). However, in a prior study of cell crowding, extrusion of live cells occurred from regions of the highest density (usually >1.6 times the normal cell density), and it was not until after extrusion that cells died of anoikis (Eisenhoffer *et al.*, 2012). In contrast, we did not observe any significant changes in cell size or density after BAPN treatment (Supplemental Figure S4), and in addition we see annexin V+ cells in the epithelium, before extrusion, and there is no apparent extrusion of live cells: labeled vascular cells are not detected in the circulation at any point during regression (Figure 6). Given that regression occurs without loss of barrier function, this suggests coordination between the phagocytes and vascular cells. Live-imaging results also support some coordination, as engulfment and extrusion appear to occur simultaneously (Supplemental Video S2). Of interest, during our attempts to live image extrusion events, it became clear that there were many more annexin V+ cells then extrusion events, suggesting that further "eat-me" signals may need to be expressed to attract the phagocytes or that the phagocytes play an active role in pulling the cells out of the epithelial tube. However, this does not rule out a role of cell density in vascular regression. In addition, a recent study in *Drosophila* suggested that an increase in tissue density could induce a competitive response due to mechanical stress, by which cells were delaminated from the imaginal wing disk epithelium in a caspase-dependent manner (Levayer *et al.*, 2016). Although the molecular mechanisms underlying this competition are not known, this effect is also consistent with our observations.

Finally, BAPN treatment may be triggering a physiological programmed tissue destruction pathway, akin to involution of other epithelial tissues, such as the mammalian uterus or breast duct after parturition or weaning, respectively. In these processes, the majority of the epithelial tissue is removed, and mechanical signaling is known to play an important role (Jorge *et al.*, 2014). This suggests that changes in the ECM could be a point of regulation during involution. In fact, older studies of mammary and Müllerian gland involution concluded that cell death follows ECM degradation (Wicha *et al.*, 1980; Ikawa *et al.*, 1984). A similar response was found in studies of angiogenesis, in which the effect of angiostatic steroids was due to breakdown of the ECM, which in turn blocked capillary growth and then induced large-scale vascular regression (Ingber *et al.*, 1986; Ingber and Folkman, 1988). Thus remodeling of the ECM may be a common first step in inducing regression of these tissues.

In summary, the present study has revealed the induction of apoptosis via changes in integrin signaling, downstream cell extrusion across basement membrane, and the participation of blood-borne phagocytic cells in vascular remodeling. Of importance, the coordination of apoptosis, extrusion, and cell clearance suggests the presence of mechanisms that maintain vessel integrity during a massive tissue-remodeling event initiated by physical changes in the ECM. It may be that BAPN treatment is causing a physical disruption, and regression is a homeostatic response to those changes. Alternatively, changes in the ECM may be the first step in a physiological regression mechanism that usually occurs locally but BAPN is stimulating on a global scale. Whereas in both cases the cause of regression would be equivalent, these studies reveal an active role of the basement membrane in the maintenance of tissue architecture. Of importance, with a 16-h visually scored assay, large transparent vessels that can be directly manipulated and imaged, as well as a number of labeling strategies that will allow purification and analysis of different cell populations (e.g., apoptotic vs. nonapoptotic vascular cells) for high-resolution studies, *Botryllus* is a potentially powerful model to study the dynamic role of the ECM and mechanotransduction in epithelial growth, homeostasis and involution.

MATERIALS AND METHODS

Animals

B. schlosseri (herein called *Botryllus*) colonies were collected from the yacht harbor in Santa Barbara, CA, and spawned and cultured in laboratory conditions at 18–20°C according to established protocols by Boyd *et al.* (1986). Colonies were staged-matched based on blastogenic stage cycles according to Lauzon *et al.* (2002). In each experiment, a replicate (defined by the variable $n = 1$) consists of three stage-matched, 3- to 6-mo-old genotypes five to eight zooids in size used in both control and experimental conditions. Regression

responses were independent of genotype or asexual stage of the samples.

Imaging

Live imaging of the vasculature of *Botryllus* colonies labeled with BSA-Alexa 594 (A13101; Thermo Fisher Scientific, Waltham, MA) was carried out using a motorized fluorescence stereomicroscope MZ16FA (Leica, Germany) as previously described (Braden *et al.*, 2014). Fixed tissue for in situ hybridization was imaged on an Olympus FluoView 1000 Spectral Confocal (Tokyo, Japan). Lipophilic staining of the vasculature labeled with CellMask Green (A37608; Thermo Fisher Scientific). Time-lapse movies ($n = 5$) taken as *z*-stacks were acquired with a Zeiss LSM 880 with Airyscan capabilities.

Lox identification and in situ hybridization

Using homology-based search tools, we identified LOX homologues in the *Botryllus* Transciptome database from Rodriguez *et al.* (2014). The contig named CAP3_round1_contig_2680 shared 43% identity to mammalian LOX1 proteins, with an *E*-value < 1*e*-39; this sequence has been deposited in the National Center for Biotechnology Information (accession number BankIt1994445 BSeq#1 KY653960). Whole-mount in situ hybridization was performed with digoxigenin-labeled probes as described by Langenbacher *et al.* (2015). A specific antisense probe for LOX1 was synthesized from PCR products using a LOX1 clone coding for a 368–base pair–specific region of the gene (primer pairs 5′-3′-: forward, GGCGTGTGGAAGTAAAGCAC; reverse, GTGAACCTGGAAACATCGCTT). We used TSA-plus detection (NEL753001KT; PerkinElmer, Waltham, MA) with a fluorescein substrate. Representative images from eight independent experiments consisting of three individual colonies per experiment are shown. Negative controls were conducted using a sense probe from the same sequence and are shown in Supplemental Figure S1.

qRT-PCR

We carried out qRT-PCR using a LightCycler 480 II (Roche, Basel, Switzerland) with LightCycler DNA Master SYBR Green I detection (12015099001; Roche). The thermocycling profile was as follows: 5 min at 95°C, and 45 cycles of 95°C for 10 s, 55°C for 10 s, and 72°C for 10 s. Primers for LOX1 were 5′-ATTTATACTGGACCAAATCAGAATCAG-3′ and 5′-CGTATGGATTTGCTACATAAGGATTAG-3′, which amplified a 244–base pair fragment of a LOX1 homologue used in this study. The template for RT-PCR was obtained by extracting mRNA from *B. schlosseri* with the Magnetic mRNA Isolation Kit (51550S; NEB), and SuperScript II Reverse Transcriptase (18064014; Invitrogen) was used to synthetize cDNA primed by Oligo dT. PCR was performed with Advantage cDNA Polymerase (639105; Clontech), and amplicones were ligated into P-GEM-T-Easy vector and sequenced through the University of California, Berkeley, Sequencing Facility. All gene expression data were normalized to elongation factor 1-α as a reference gene, reported as relative expression using the $2^{-\Delta\Delta Ct}$ method (Livak and Schmittgen, 2001), and analyzed in triplicate (both technical and biological).

BAPN treatment

To inhibit LOX1 activity, BAPN (150105; MP Biomedicals, Santa Ana, CA) was diluted in 500 ml of FSW to the concentrations tested (50, 100, 200, 400, and 800 µM). *Botryllus* colonies were allowed to soak in either a FSW control or the BAPN-containing solution for 16 h at 18–20°C before measurements of vascular regression ($n = 15$). To test the reversibility of vascular regression, colonies were first treated with BAPN (as described) for 16 h at 18–20°C and then returned to normal seawater and regrowth monitored visually ($n = 10$). To assess whether the cells were disturbed by BAPN treatment, colonies were incubated for 8 h and then fixed and stained with phalloidin and 4′,6-diamidino-2-phenylindole and compared with control colonies (six control and six treated conditions).

Vascular and phagocytic cell labeling

Vascular cell labeling was achieved as previously described (Braden *et al.*, 2014). Briefly, adult *Botryllus* colonies were injected with 1µl of 0.1 µg/ml Alexa Fluor 647–conjugated BSA to label the cells of the vascular tissue. Phagocytic cell labeling was achieved using pHrodo Green *Escherichia coli* BioParticles (P35366; Thermo Fisher Scientific) as previously described (Lauzon *et al.*, 2013). Double-positive cells (yellow) were manually counted from each field of view and normalized by the number of fields per sample (five for each of control conditions and BAPN treatment conditions). Statistical analysis was performed using Student's *t* test; $*p = 0.05$.

Transmission electron microscopy

Colonies were anesthetized with MS-222 (tricaine; ethyl 3-animobenzoate methanesulfonate salt; 103106, MP Biomedicals) for ~5 min in FSW and fixed with 1.5% glutaraldehyde buffered with 1.6% sodium chloride and 0.2 M sodium cacodylate (pH 7.2) on ice. After soaking overnight in 0.1 M sodium cacodylate buffer, specimens were quickly rinsed with fresh buffer and postfixed in cold with 2% OsO_4 buffered with 0.2 M sodium cacodylate. After being washed with water, the samples were en-bloc stained with uranyl acetate, then dehydrated and embedded in Epon. Thin sections were stained in uranyl acetate and lead citrate and examined using a JEOL 1234 electron microscope. Representative images from seven controls and six BAPN-treated colonies (3–6 mo old) are shown.

Annexin V assays

For annexin V labeling (1988549001; Roche), *Botryllus* colonies were injected with annexin V (1 µl per adult colonial systems with five to eight zooids, aged 3–6 mo), followed by treatment with BAPN (400 µM) for 16 h. Representative images from six controls and six BAPN-treated colonies are shown. Annexin V+ cells were manually counted from each field of view and normalized by the number of fields per sample. Statistical analysis was performed using Student's *t* test; $*p = 0.001$.

Second-harmonic imaging of collagen

For imaging of collagen fibers of *Botryllus,* bodies and vasculature colonies were fixed with Carnoy's solution (6:3:1 of 100% ethanol:$CHCl_3$:glacial acetic acid) at 0-, 8-, and 16-h time points for both control and BAPN-treated samples. After 3 h of fixation, colonies were bleached with 6% hydrogen peroxide to eliminate autofluorescence from pigment cells. SHI was performed as described by Schenke-Layland (2008). Briefly, imaging of *Botryllus* vessels at an excitation wavelength of 800 nm revealed fibrous collagen structures. Emission was collected using an Olympus FluoView 1000 MPE upright microscope that features three visible confocal laser lines, a Mai Tai pulsed two-photon femtosecond laser for two-photon imaging, a scanning *XY*-stage, and a standard motorized *Z*-stage. All samples were imaged using the same settings as the control at 0 h. To quantify the intrinsic fluorescence signal of collagenous structures, *z*-stacks were rendered, and the intensity of the signal was calculated by measuring the mean intensity of the vessel using ImageJ. All samples were normalized and compared with the control at 0 h ($n = 6$); the SD of the mean of the intensity was calculated using Microsoft Excel for each data set.

Flow cytometry and inhibitor studies

Botryllus colonies (3–6 mo old) were injected with 1 µl of BSA–Alexa Fluor 488 conjugate (1 mg/ml in phosphate-buffered saline [PBS]) 24 h before drug treatment to label vascular cells. The colonies were subsequently treated with BAPN, FAKI14 (CAS 4506-66-5; 50 µM), Raf kinase inhibitor (CAS 303727-31-3; 10 µM), or a vehicle control (six per condition). FAK and Raf inhibitor doses were determined empirically and represent the lowest concentration that gave maximum but reversible regression in dose–response curves. Treated colonies were kept in a humidity chamber for 4 h, at which time, regression was visible. Next single-cell preparations were made by manually dissociating colonies in FSW, followed by filtering through progressive 70- and 40-µm filters. Fixation was achieved by adding 100 µl of 16% formaldehyde solution to 1 ml of cell suspension (1.5% final concentration) and incubating at room temperature for 10 min. The cells were washed with PBS and then resuspended in 1 ml of –20°C 100% methanol and placed on ice for 30 min. The cells were rehydrated in two sequential washes with 2 ml of PBS. Antibody staining was performed for 30 min at room temperature in PBS containing 1% immunoglobulin G (IgG)-free BSA. Anti–phospho FAK Y397 (clone 31H5L17; 700255; Thermo Fisher) was diluted 1:200. Brilliant Violet 421 donkey anti-rabbit IgG antibody was used as secondary at a 1:400 dilution. There is a single FAK clone in the *Botryllus* transcriptome database with nearly 100% overlap with the conserved phosphorylation site, and a Western blot reveals a single band of the expected size (~125 kDa; Supplemental Figure S5E). For annexin V labeling (1988549001; Roche), vascular-labeled *Botryllus* colonies were injected with annexin V (1 µl per system), followed by treatment with BAPN (400 µM) for 16 h. Individual colonies were manually dissociated in FSW before filtration through 40-µm mesh, and flow cytometry analysis was carried out as described in the text. The percentage of annexin V+ vascular cells with or without BAPN treatment was compared across multiple colonies (n = 10). Statistical analysis was performed using Student's t test; *p = 0.002 (high significance vs. control).

pFAK Western blot analysis

For anti–phospho-Y397-FAK Western blots, each *Botryllus* system was lysed in 300 µl of Rubinfeld's Lysis Buffer (20 mM Tris, pH 8.0, 140 mM NaCl, 1% Triton X-100, 10% glycerol, 1 mM ethylene glycol tetraacetic acid, 1.5 mM $MgCl_2$, 1 mM Na_3VO_4, 50 mM NaF, 1 mM dithiothreitol) with protease and phosphatase inhibitors (Roche). Binding of anti–phospho-Y397-FAK antibody (700255; Thermo Fisher Scientific) was performed overnight at 4°C, and bound proteins were then pulled down using protein G–agarose beads. Controls are protein G beads only. Immunoprecipitated proteins were separated by SDS–PAGE, transferred to a nitrocellulose membrane, and detected using anti–phospho-Y397-FAK antibody (700255; Thermo Fisher Scientific).

ACKNOWLEDGMENTS

We thank Leanne Jones, Herb Waite, Robert Mecham, and anonymous reviewers for helpful discussions and input and Hayley Simon and Darius Martins for assistance with the experiments with BAPN recovery and SHI of collagen fibers. We also thank Mike Caun for expert care of the De Tomaso laboratory mariculture facility and Neeraj Gohad and Carl Zeiss Microscopy for technical assistance in the live-imaging experiments. We acknowledge funding through National Institutes of Health Grants R01-AG037699 and R01-AI401588, Cottage Hospital Grants 243, 297, and 303 to A.W.D., through National Science Foundation Award CMMI-1254893 a CAREER Award and a Scialog-Molecules Come to Life Grant from the Gordon and Betty Moore Foundation to M.T.V., and a grant from the G. Harold and Leila Y. Mathers Foundation to A.W.D. and M.T.V. The NRI-MCDB Microscopy Facility and the Spectral Laser Scanning Confocal are supported by the Office of the Director, National Institutes of Health, under Award S10OD010610. D.R. was supported by a California Institute for Regenerative Medicine Postdoctoral Fellowship and S.W.B. by the Santa Barbara Tri-Counties Blood Bank and Otis Williams Postdoctoral Fellowships.

REFERENCES

Bignon M, Pichol-Thievend C, Hardouin J, Malbouyres M, Brechot N, Nasciutti L, Barret A, Teillon J, Guillon E, Etienne E, *et al.* (2011). Lysyl oxidase-like protein-2 regulates sprouting angiogenesis and type IV collagen assembly in the endothelial basement membrane. Blood 118, 3979–3989.

Boyd HC, Brown SK, Harp JA, Weissman IL (1986). Growth and sexual-maturation of laboratory-cultured Monterey Botryllus-Schlosseri. Biol Bull 170, 91–109.

Braden BP, Taketa DA, Pierce JD, Kassmer S, Lewis DD, De Tomaso AW (2014). Vascular regeneration in a basal chordate is due to the presence of immobile, bi-functional cells. PLoS One 9, e95460.

Brown NH (2011). Extracellular matrix in development: insights from mechanisms conserved between invertebrates and vertebrates. Cold Spring Harb Perspect Biol 3, a005082.

Brunetti R, Burighel P (1969). Sviluppo dell'apparato vascolare coloniale in Botryllus schlosseri (Pallas). Pubbl Staz Zool Napoli 37, 137–148.

Burighel P, Brunetti R (1971). The circulatory system in the blastozooid of the colonial ascidian Botryllus schlosseri (Pallas). Boll Zool 38, 273–289.

Campagnola P (2011). Second harmonic generation imaging microscopy: applications to diseases diagnostics. Anal Chem 83, 3224–3231.

Chen JY, Tsai PJ, Tai HC, Tsai RL, Chang YT, Wang MC, Chiou YW, Yeh ML, Tang MJ, Lam CF, *et al.* (2013). Increased aortic stiffness and attenuated lysyl oxidase activity in obesity. Arterioscler Thromb Vasc Biol 33, 839–846.

Chen SZ, Xu X, Ning LF, Jiang WY, Xing C, Tang QQ, Huang HY (2015). miR-27 impairs the adipogenic lineage commitment via targeting lysyl oxidase. Obesity (Silver Spring) 23, 2445–2453.

Chen X, Nadiarynkh O, Plotnikov S, Campagnola PJ (2012). Second harmonic generation microscopy for quantitative analysis of collagen fibrillar structure. Nat Protoc 7, 654–669.

Cox G, Kable E, Jones A, Fraser I, Manconi F, Gorrell MD (2003). 3-Dimensional imaging of collagen using second harmonic generation. J Struct Biol 141, 53–62.

Cox TR, Rumney RM, Schoof EM, Perryman L, Hoye AM, Agrawal A, Bird D, Latif NA, Forrest H, Evans HR, *et al.* (2015). The hypoxic cancer secretome induces pre-metastatic bone lesions through lysyl oxidase. Nature 522, 106–110.

Delsuc F, Brinkmann H, Chourrout D, Philippe H (2006). Tunicates and not cephalochordates are the closest living relatives of vertebrates. Nature 439, 965–968.

Di Maio A, Setar L, Tiozzo S, De Tomaso AW (2015). Wnt affects symmetry and morphogenesis during post-embryonic development in colonial chordates. Evodevo 6, 17.

Eisenhoffer GT, Loftus PD, Yoshigi M, Otsuna H, Chien CB, Morcos PA, Rosenblatt J (2012). Crowding induces live cell extrusion to maintain homeostatic cell numbers in epithelia. Nature 484, 546–549.

Frisch SM, Francis H (1994). Disruption of epithelial cell-matrix interactions induces apoptosis. J Cell Biol 124, 619–626.

Gasparini F, Longo F, Manni L, Burighel P, Zaniolo G (2007). Tubular sprouting as a mode of vascular formation in a colonial ascidian (Tunicata). Dev Dynam 236, 719–731.

Guo W, Giancotti FG (2004). Integrin signalling during tumour progression. Nat Rev Mol Cell Biol 5, 816–826.

Guo W, Liu R, Bhardwaj G, Ma AH, Changou C, Yang JC, Li Y, Feng C, Luo Y, Mazloom A, *et al.* (2013). CTA095, a novel Etk and Src dual inhibitor, induces apoptosis in prostate cancer cells and overcomes resistance to Src inhibitors. PLoS One 8, e70910.

Harunaga JS, Doyle AD, Yamada KM (2014). Local and global dynamics of the basement membrane during branching morphogenesis require protease activity and actomyosin contractility. Dev Biol 394, 197–205.
Hochwald SN, Nyberg C, Zheng M, Zheng D, Wood C, Massoll NA, Magis A, Ostrov D, Cance WG, Golubovskaya VM (2009). A novel small molecule inhibitor of FAK decreases growth of human pancreatic cancer. Cell Cycle 8, 2435–2443.
Ihara S, Hagedorn EJ, Morrissey MA, Chi Q, Motegi F, Kramer JM, Sherwood DR (2011). Basement membrane sliding and targeted adhesion remodels tissue boundaries during uterine-vulval attachment in Caenorhabditis elegans. Nat Cell Biol 13, 641–651.
Ikawa H, Trelstad RL, Hutson JM, Manganaro TF, Donahoe PK (1984). Changing patterns of fibronectin, laminin, type IV collagen, and a basement membrane proteoglycan during rat Mullerian duct regression. Dev Biol 102, 260–263.
Ingber D, Folkman J (1988). Inhibition of angiogenesis through modulation of collagen metabolism. Lab Invest 59, 44–51.
Ingber DE, Madri JA, Folkman J (1986). A possible mechanism for inhibition of angiogenesis by angiostatic steroids: induction of capillary basement membrane dissolution. Endocrinology 119, 1768–1775.
Isabella AJ, Horne-Badovinac S (2015). Dynamic regulation of basement membrane protein levels promotes egg chamber elongation in Drosophila. Dev Biol 406, 212–221.
Jorge S, Chang S, Barzilai JJ, Leppert P, Segars JH (2014). Mechanical signaling in reproductive tissues: mechanisms and importance. Reprod Sci 21, 1093–1107.
Kagan HM (2000). Intra- and extracellular enzymes of collagen biosynthesis as biological and chemical targets in the control of fibrosis. Acta Trop 77, 147–152.
Langenbacher AD, De Tomaso AW (2016). Temporally and spatially dynamic germ cell niches in Botryllus schlosseri revealed by expression of a TGF-beta family ligand and vasa. Evodevo 7, 9.
Langenbacher AD, Rodriguez D, Di Maio A, De Tomaso AW (2015). Whole-mount fluorescent in situ hybridization staining of the colonial tunicate Botryllus schlosseri. Genesis 53, 194–201.
Lauzon RJ, Brown C, Kerr L, Tiozzo S (2013). Phagocyte dynamics in a highly regenerative urochordate: insights into development and host defense. Dev Biol 374, 357–373.
Lauzon RJ, Ishizuka KJ, Weissman IL (2002). Cyclical generation and degeneration of organs in a colonial urochordate involves crosstalk between old and new: a model for development and regeneration. Dev Biol 249, 333–348.
Levayer R, Dupont C, Moreno E (2016). Tissue crowding induces caspase-dependent competition for space. Curr Biol 26, 670–677.
Li H, Zhou Y, Zhao A, Qiu Y, Xie G, Jiang Q, Zheng X, Zhong W, Sun X, Zhou Z, Jia W (2013). Asymmetric dimethylarginine attenuates serum starvation-induced apoptosis via suppression of the Fas (APO-1/CD95)/JNK (SAPK) pathway. Cell Death Dis 4, e830.
Liu SB, Ikenaga N, Peng ZW, Sverdlov DY, Greenstein A, Smith V, Schuppan D, Popov Y (2015). Lysyl oxidase activity contributes to collagen stabilization during liver fibrosis progression and limits spontaneous fibrosis reversal in mice. FASEB J 30, 1599–1609.
Livak KJ, Schmittgen TD (2001). Analysis of relative gene expression data using real-time quantitative PCR and the 2(-Delta Delta C(T)) method. Methods 25, 402–408.
Macara IG, Guyer R, Richardson G, Huo Y, Ahmed SM (2014). Epithelial homeostasis. Curr Biol 24, R815–R825.
Macias H, Hinck L (2012). Mammary gland development. Wiley Interdiscip Rev Dev Biol 1, 533–557.
Maki JM, Rasanen J, Tikkanen H, Sormunen R, Makikallio K, Kivirikko KI, Soininen R (2002). Inactivation of the lysyl oxidase gene Lox leads to aortic aneurysms, cardiovascular dysfunction, and perinatal death in mice. Circulation 106, 2503–2509.
Morrissey MA, Sherwood DR (2015). An active role for basement membrane assembly and modification in tissue sculpting. J Cell Sci 128, 1661–1668.
Morse EM, Brahme NN, Calderwood DA (2014). Integrin cytoplasmic tail interactions. Biochemistry 53, 810–820.
Pastor-Pareja JC, Xu T (2011). Shaping cells and organs in Drosophila by opposing roles of fat body-secreted collagen IV and perlecan. Dev Cell 21, 245–256.
Patricolo E, Ferrarella A (1973). Histochemical and biochemical studies on the collagen of the tunica of Ciona intestinalis. Riv Biol 66, 115–134.
Rodriguez D, Sanders EN, Farell K, Langenbacher AD, Taketa DA, Hopper MR, Kennedy M, Gracey A, De Tomaso AW (2014). Analysis of the basal chordate Botryllus schlosseri reveals a set of genes associated with fertility. BMC Genomics 15, 1183.
Rozario T, DeSimone DW (2010). The extracellular matrix in development and morphogenesis: a dynamic view. Dev Biol 341, 126–140.
Schenke-Layland K (2008). Non-invasive multiphoton imaging of extracellular matrix structures. J Biophotonics 1, 451–462.
Senger DR, Davis GE (2011). Angiogenesis. Cold Spring Harb Perspect Biol 3, a005090.
Shapiro IM, Kolev VN, Vidal CM, Kadariya Y, Ring JE, Wright Q, Weaver DT, Menges C, Padval M, *et al*. (2014). Merlin deficiency predicts FAK inhibitor sensitivity: a synthetic lethal relationship. Sci Transl Med 6, 237–268.
Smith-Mungo LI, Kagan HM (1998). Lysyl oxidase: properties, regulation and multiple functions in biology. Matrix Biol 16, 387–398.
Tiozzo S, Voskoboynik A, Brown FD, De Tomaso AW (2008). A conserved role of the VEGF pathway in angiogenesis of an ectodermally-derived vasculature. Dev Biol 315, 243–255.
Vizzini A, Arizza V, Cervello M, Camma-rata M, Gambino R, Parrinello N (2002). Cloning and expression of a type IX-like collagen in tissues of the ascidian Ciona intestinalis. Biochim Biophys Acta 1577, 38–44.
Wang J, Zhu Y, Tan J, Meng X, Xie H, Wang R (2016). Lysyl oxidase promotes epithelial-to-mesenchymal transition during paraquat-induced pulmonary fibrosis. Mol Biosyst 12, 499–507.
Wicha MS, Liotta LA, Vonderhaar BK, Kidwell WR (1980). Effects of inhibition of basement membrane collagen deposition on rat mammary gland development. Dev Biol 80, 253–256.
Wu Z, Wu Y, Tian Y, Sun X, Liu J, Ren H, Liang C, Song L, Hu H, Wang L, Jiao B (2013). Differential effects of miR-34c-3p and miR-34c-5p on the proliferation, apoptosis and invasion of glioma cells. Oncol Lett 6, 1447–1452.
Zang W, Wang T, Wang Y, Li M, Xuan X, Ma Y, Du Y, Liu K, Dong Z, Zhao G (2014). Myricetin exerts anti-proliferative, anti-invasive, and pro-apoptotic effects on esophageal carcinoma EC9706 and KYSE30 cells via RSK2. Tumour Biol 35, 12583–12592.